ELSEVIER

Earth and Planetary Science Letters 194 (2001) 83–95

EPSL

www.elsevier.com/locate/epsl

# Seismic evidence for a rapidly varying compositional anomaly at the base of the Earth's mantle beneath the Indian Ocean

Lianxing Wen

*Department of Geosciences, State University of New York at Stony Brook, Stony Brook, NY 11794, USA*

Received 23 July 2001; received in revised form 11 October 2001; accepted 11 October 2001

**Abstract**

Seismic observations recorded by an African seismic array reveal a low velocity anomaly at the base of the mantle beneath the Indian Ocean, with steeply dipping edges, rapidly varying thicknesses and geometries, and anomalously low shear wave velocities decreasing from −2% at 200 km above the core–mantle boundary to −9% to −12% at the core–mantle boundary (relative to the preliminary reference Earth model). These characteristics unambiguously suggest that it is a compositional anomaly and its velocity structures can be well explained by partial melt driven by a compositional change produced early in the Earth's history. This chemical anomaly geographically coincides with the DUPAL geochemical anomaly observed in island volcanoes around the Indian Ocean and may provide an explanation for its distinctive isotope characteristics observed at the Earth's surface. 

*Keywords:* geochemical anomalies; partial melting; core–mantle boundary; Earth; differentiation

## 1. Introduction

Variations of chemistry inside the Earth are expected from early accretion and chemical differentiation. Identifying chemically distinct reservoirs is important not only for understanding the evolution and differentiation of the Earth, but also for studying mantle convection and geochemistry, since those chemical reservoirs are part of the Earth's circulation system [1–3] and possibly contribute to or affect geochemical signatures [4] and geodynamic observations [5] at the surface of the Earth. Many studies suggest that there may exist chemical anomalies in the lower mantle [6–15], especially in the lowermost mantle [9–15]. Resolving the existence of these chemical anomalies, however, remains challenging [9–17]. Recently, Wen et al. [18] show that resolving structural features of a seismic anomaly is crucial to distinguishing a chemical anomaly from a thermal anomaly. They report seismic evidence for a unique 300 km thick layer at the base of the mantle beneath the south Atlantic Ocean, with a steeply dipping edge, anomalously low shear wave velocities linearly decreasing from −2% (top) to −10% to −12% (bottom) and a maximum P velocity decrease of −3% relative to the preliminary reference Earth model (PREM) [19]. They also suggest that the seismic characteristics and structural features of that boundary layer can be best explained by partial melt driven by a compositional change produced early in the Earth's history and a vertical thermal gradient within

*E-mail address:* lianxing.wen@sunysb.edu (L. Wen).

0012-821X/01/$ – see front matter 
PII: S0012-821X(01)00550-7

the layer. Here, I report seismic evidence for a seismic anomaly at the base of the Earth's mantle beneath the Indian Ocean, which appears geographically connected to the boundary layer beneath the south Atlantic Ocean. From extensive waveform modeling of seismic waves recorded in a dense African array, I am able to constrain not only the velocity variation and geometry, but also the geographic extent and variation of this seismic anomaly. The seismic anomaly has a maximum thickness of 200 km, shear velocity reductions from −2% (top) to −9% to −12% (bottom) (with respect to PREM), steeply dipping edges and rapidly varying thicknesses and geometries. Its structural features and seismic characteristics unambiguously confirm that it is a compositional anomaly.

## 2. Seismic observations and models

In this section, I present seismic observations associated with this anomaly beneath the Indian Ocean, and detailed waveform modeling and travel time analysis of these observations. The seismic technique and detailed discussions of SHdiff propagation through heterogeneous structures near the core–mantle boundary are presented in a separate paper [20]. I perform travel time analysis and waveform modeling for seismic waves propagating near and along the core–mantle boundary (S, ScS, Sdiff and Pdiff) and travel time analysis for the core phase SKS (Fig. 1c). My dataset consists of displacements recorded by a dense temporary seismic array deployed in southern Africa from April 1997 to July 1999 (Fig. 1a). I search re-

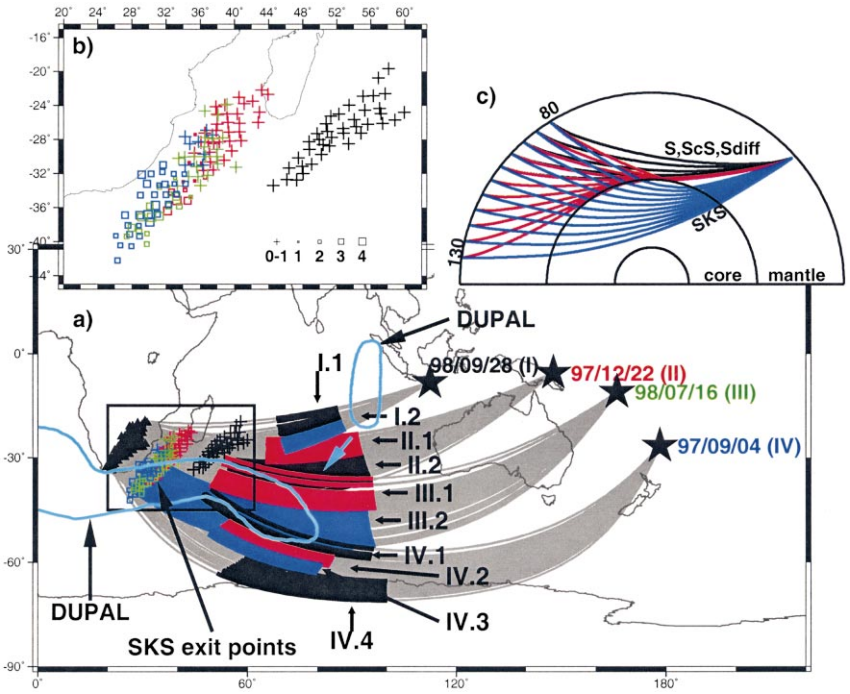


Fig. 1. (a) Great-circle paths from four events (stars and Table 1) to the southern African array (triangles), with the portions of raypath sampling the lowermost mantle shaded. Sections are divided based on the appearance of observed seismograms, with those of each section shown in Figs. 2, 3, 5, and 6. The seismic anomaly emerges in section I.2 in the north and disappears in section IV.4 in the south. DUPAL anomaly maxima [26] are also plotted as light blue contours. DUPAL maxima for the 90-east ridge (top right contour) are samples of old hotspot traces and their origin should be further southwest as indicated by the light blue arrow [26]. The box indicates the geographic locations where SKS phases exit the core–mantle boundary in the receiver side with travel time anomalies plotted (see panel b for an enlarged version). (b) SKS travel time delays plotted on their exit points. The travel time pick error is 1 s. The observations are color-coded in the same way as the events are labeled in panel a. (c) Raypaths of S, ScS, Sdiff and SKS phases.

Table 1
Event list (after relocation)

| No. | Origin | Latitude | Longitude | Depth (km) |
|---|---|---|---|---|
| 980928 | 98/09/28 13:34:27 | −8.19 | 112.41 | 152 |
| 971222 | 97/12/22 02:05:46 | −5.49 | 147.87 | 179 |
| 980716 | 98/07/16 11:56:30 | −11.04 | 166.16 | 110 |
| 970904 | 97/09/04 04:23:33 | −26.57 | 178.34 | 625 |

corded ground displacements for earthquakes in the Fiji subduction zone and select four earthquakes based on the sampling coverage and the simplicity of the earthquake source (Fig. 1a, Table 1). The observations of these four earthquakes provide a good sampling coverage for the lowermost mantle beneath the Indian Ocean (Fig. 1a) and bracket the emergence of the anomaly in the north (section I.2, Fig. 1a) and its disappearance in the south (section IV.4, Fig. 1a). I present seismic observations and detailed seismic modeling from north (section I.1) to south (section IV.4).

The observations sampling section I.1 show no evidence for an anomalous seismic structure throughout the lower mantle. In fact, both the tangential (light traces, Fig. 2a) and radial (light traces, Fig. 2b) displacements sampling this section can be explained by PREM synthetics (light traces, Fig. 2c,d). ScS phases sampling section I.2 (heavy traces and phases labeled as ScS, Fig. 2a,b), however, arrive late compared to the PREM predictions. The ScS travel time delays are caused by a localized low velocity structure at the base of the mantle, as both S and SKS phases (heavy traces, labeled as S and SKSac, Fig. 2a–d) can be explained by PREM. Because of the trade-offs between thickness of the layer and magnitude of the shear velocity reduction, I adopt a shear velocity reduction of −12%, a value obtained from waveform modeling of the observations sampling section II.1, and search for the thickness of the layer. The ScS phases, on average, can be explained by a 15 km thick basal layer (heavy traces, Fig. 2c,d). This thickness is also consistent with SH observations from pre-diffracted to diffracted distances from other events sampling the same section. This basal layer does not extend to the west where SKS phases exit the core–mantle boundary, as SKS phases for this event show small travel time delays across the array (black crosses, Fig. 1a,b).

SHdiff observations are used to constrain the seismic structures further south of the lowermost mantle (Fig. 1a, sections II.1–IV.4). SHdiff travel time and waveform are sensitive to detailed seismic velocity variation and laterally dipping structure in the lowermost mantle, where these phases propagate horizontally (Fig. 1c) [18,20]. The observed travel time and waveform complexities require such large velocity reductions at the base of the mantle that direct arrivals propagate through the top of the low velocity zones. The first direct arrival is determined by the thickness of the layer and seismic waveforms are controlled by the geometry and detailed velocity distribution of the seismic structure [18,20]. The observations recorded for events II–IV exhibit rapid variations of travel time and waveform complexity across small distances (Figs. 3, 5 and 6). The changes of Sdiff travel time delays are also accompanied by the variations of waveform complexities (Figs. 3 and 6). The waveform complexities and travel time delays are caused by anomalous seismic structures in the lowermost mantle, as other possible causes can be confidently eliminated. (1) They cannot be the result of seismic heterogeneities in the source-side mantle. As the observed SH phases propagate over almost identical raypaths in the source-side mantle, seismic heterogeneities in the source-side mantle should result in uniform time delays and similar waveforms across the array. (2) The waveform complexities cannot be caused by complicated earthquake sources for two reasons: (a) the waveforms observed at other GSN stations display simple pulse-like shapes indicating simple source time functions; and (b) the waveform complexities in the different sections for a same event are markedly different. (3) Near-station effects and receiver-side mantle structure appear to contribute little to the observed time delays across the seismic array, as the SKS phases, which sample further west of the African mantle, either exhibit small travel time delays or show no correlations or anti-correlations with SHdiff travel time delays (Fig. 1b). SKS phases observed for event I show no travel time delays (Figs. 1a and

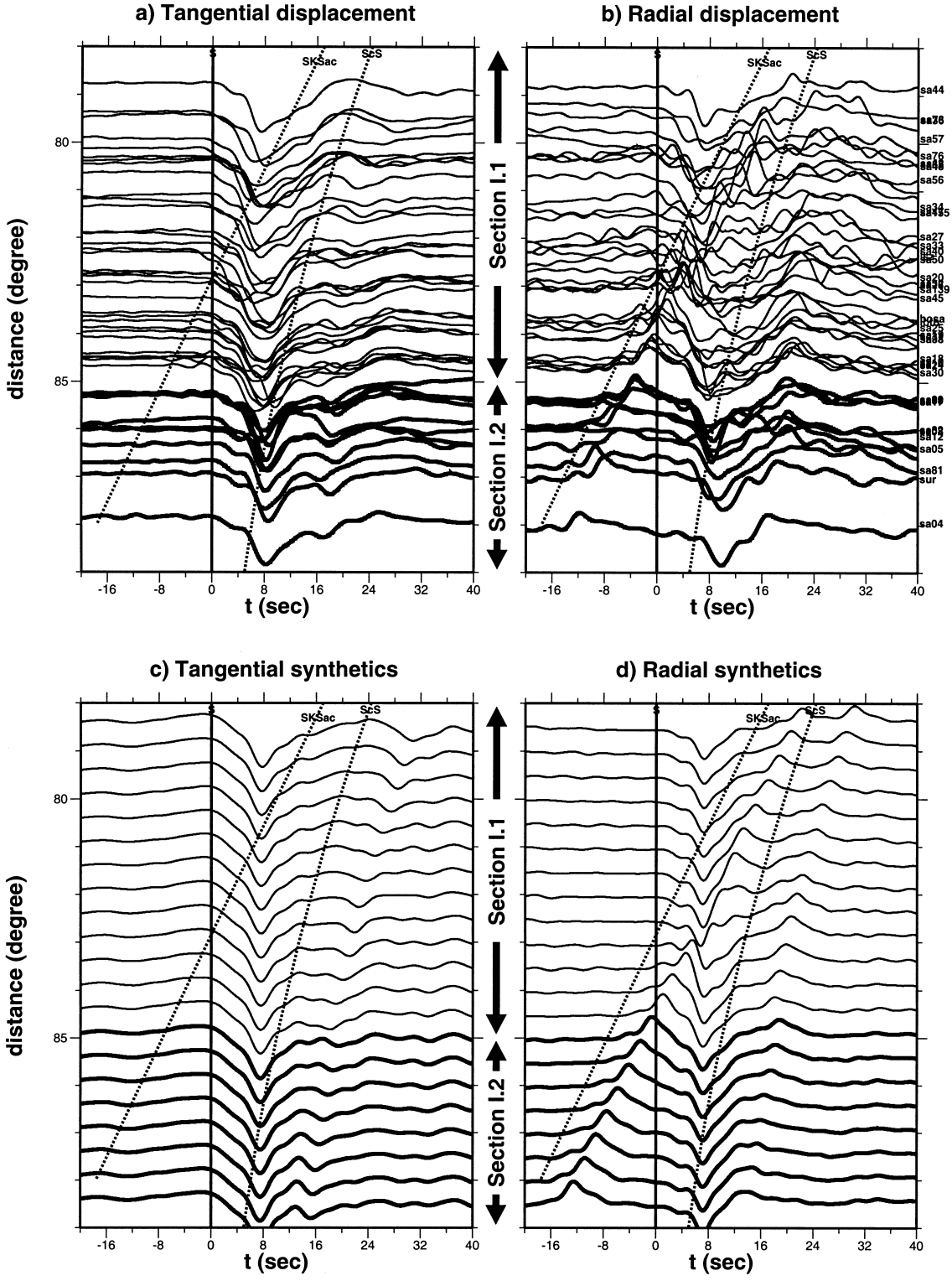
a) Tangential displacement
b) Radial displacement
c) Tangential synthetics
d) Radial synthetics
S
SKSac
ScS
distance (degree)
80
85
Section I.1
Section I.2
-16
-8
0
8
16
24
32
40
t (sec)
sa44
sa57
sa56
sa27
sa45
sa30
sa05
sa81
sur
sa04

Fig. 2. Observed broadband tangential (a) and radial (b) displacements for event 98/09/28 (I), along with synthetics from two models (c, d). The light and heavy traces are for sections I.1 and I.2, respectively (see Fig. 1a for geographic locations). Traces are aligned along SH arrivals and dashed lines are theoretical arrivals of ScS and SKS phases predicted based on PREM. All phases in synthetics for section I.1 (light traces; c, d) and SKS phases for section I.2 (heavy traces labeled as SKSac; c, d) are calculated based on PREM, whereas S and ScS phases in the synthetics for section I.2 (heavy traces labeled as S and ScS; c, d) are calculated based on a model with a 15 km thick basal layer with a shear velocity reduction of −12% (with respect to PREM) embedded within PREM. Note that there are also variations in ScS travel times in section I.2, azimuthally increasing from north to south.
←

2a). Travel time delays are consistently observed for the SKS phases exiting south of (32°S, 35°E) for events II–IV (Fig. 1b), but the changes of SKS travel times across the seismic array do not coincide or correlate with the changes of Sdiff travel times for events II–III. For event IV, large travel time delays are observed for Sdiff phases in section IV.1 (Fig. 6a), while SKS phases show no travel time delays (Fig. 1a). On the other hand, SKS travel time delays are observed in section IV.4 (Fig. 1a), while Sdiff phases show no travel time delays across the array (Fig. 6g). The SKS and Sdiff travel time delays also anti-correlate with each other for sections IV.2 and IV.3 (Figs. 1a and 6c,e). The SKS travel time delays instead correlate with geographic locations of SKS exit points from event to event, indicating they are caused by the seismic structures in the lowermost

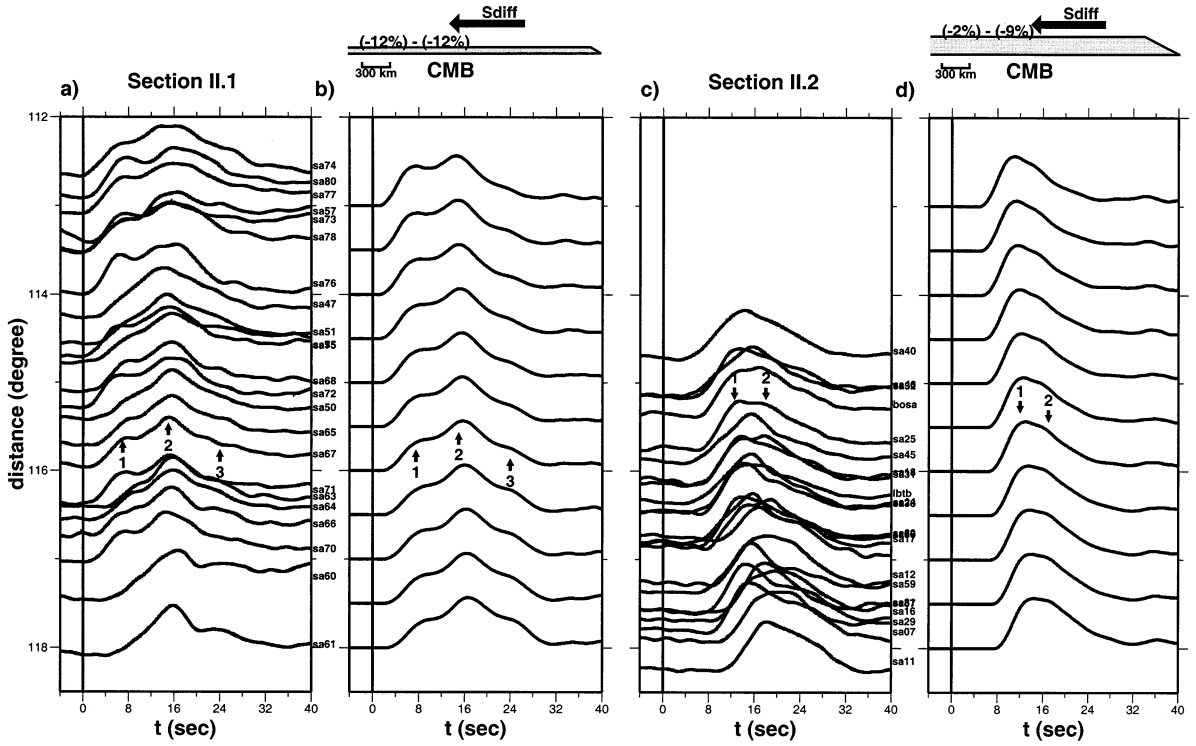


Fig. 3. Observed tangential broadband displacements (a, c) and synthetics (b for a, d for c) for event 97/12/22 (II) (see Fig. 1a for geographic locations of sections II.1 and II.2). Synthetics are calculated using a 67 km thick layer at the bottom of the mantle with a velocity reduction of −12% (b) and a 200 km thick layer with a negative velocity gradient from −2% (top) to −9% (bottom) (d). Model geometries are plotted at the top of panels b and d. Note the rapid change of travel time and waveform features between the two groups of observations across a small distance (see Fig. 1a). Traces are aligned along their theoretical predicted direct SH arrivals ($t=0$) based on PREM.

mantle at those SKS exit points. Indeed, the magnitude of SKS travel times is consistent with results from other studies in this region using other phases [21,22].

The tangential displacements sampling section II.1 show a linearly increasing travel time delay of 4 s from 112° to 118°, and multiple phases following the first arrivals (phases labeled as 1, 2, 3, Fig. 3a). Large velocity reductions are required to generate these strong multiples. In order to explain the observed travel time of the direct arrivals in the presence of large low velocity reductions, the seismic anomaly also needs to be confined within 67 km of the lowermost mantle. In fact, a 67 km thick basal layer with a shear velocity reduction of −12% explains both the waveforms and travel times well (Fig. 3b). The phases 2 and 3 are multiple reflections inside the 67 km layer. The strong phase 3 is generated by the large impedance contrast across the top of the layer. The observed travel times and waveforms tightly constrain seismic velocities and model geometry. Models with a smaller thickness and a larger velocity reduction predict small travel time delays and non-pulse-like multiples (see Fig. 4a for an example), different from the observations (Fig. 3a); models with a larger thickness, or models with a small negative velocity gradient embedded with a thin ultra-low velocity zone, predict travel times larger than those observed (see Fig. 4d for an example and cf. Fig. 3a). The observations sampling section II.2, on the other hand, show a linearly increasing travel time delay of 13 s and exhibit waveform broadening and a triplicated phase (phase 2, Fig. 3c) following the first arrivals (Fig. 3c). Both the observed travel time and waveform features can be explained by a 200 km thick basal layer with a negative velocity gradient from −2%

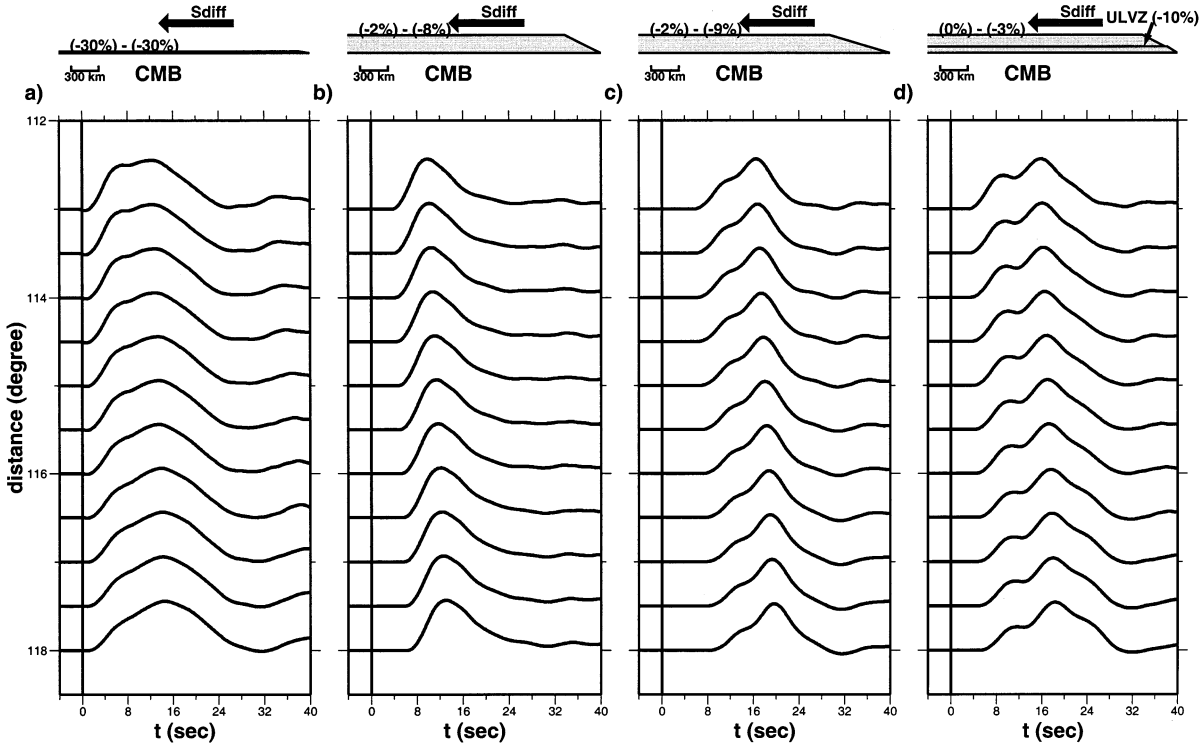


Fig. 4. Synthetic seismograms for four models selected to illustrate the sensitivity of model parameters. (a) A 20 km thick layer with a shear velocity reduction of −30%. (b) A 200 km thick layer with a negative shear velocity gradient from −2% to −8%. (c) A 200 km thick layer with a negative shear velocity gradient from −2% to −9% and a shallowly dipping edge. (d) A 200 km thick layer with a negative velocity gradient of −3% embedded with a ultra-low velocity zone with a shear velocity reduction of −10%.

(top) to −9% (bottom) and a steeply dipping edge (Fig. 3d). These observations cannot be explained by models with a smaller velocity gradient, or a shallower dipping edge, or a smaller negative velocity gradient embedded with thin ultra-low velocity zones. Models with a negative velocity gradient involving less maximum velocity reduction than −9% at the core–mantle boundary cannot generate the phase 2 and waveform broadening as those sampling section II.2 (see an example in Fig. 4b and cf. Fig. 3c); models with a shallowly dipping edge cannot predict pulse-like waveform features observed in section II.2 (see an example in Fig. 4c and cf. Fig. 3c); models with a small negative velocity gradient embedded with a thin ultra-low velocity zone predict smaller travel time delays than those sampling section II.2 (see an example in Fig. 4d and cf. Fig. 3c) and different waveform features from observations (Fig. 3c).

Seismic observations for event III bridge the sampling between section II.2 in the north and section IV.1 in the south (Fig. 1a). Tangential displacements observed in section III.1 (Fig. 5a) can be explained by the model used in section II.2 (Fig. 5b), suggesting that the seismic anomaly does not vary significantly between sections II.2 and III.1. The travel time delays decrease for those in sampling section III.2 (Fig. 5c), suggesting a decrease of thickness of the seismic anomaly. The travel times and waveforms in this section can both be explained with an 180 km thick layer with the same shear velocity gradient in section III.1 (Fig. 5d). The waveform features are consistent with steeply dipping edges in both these sections.

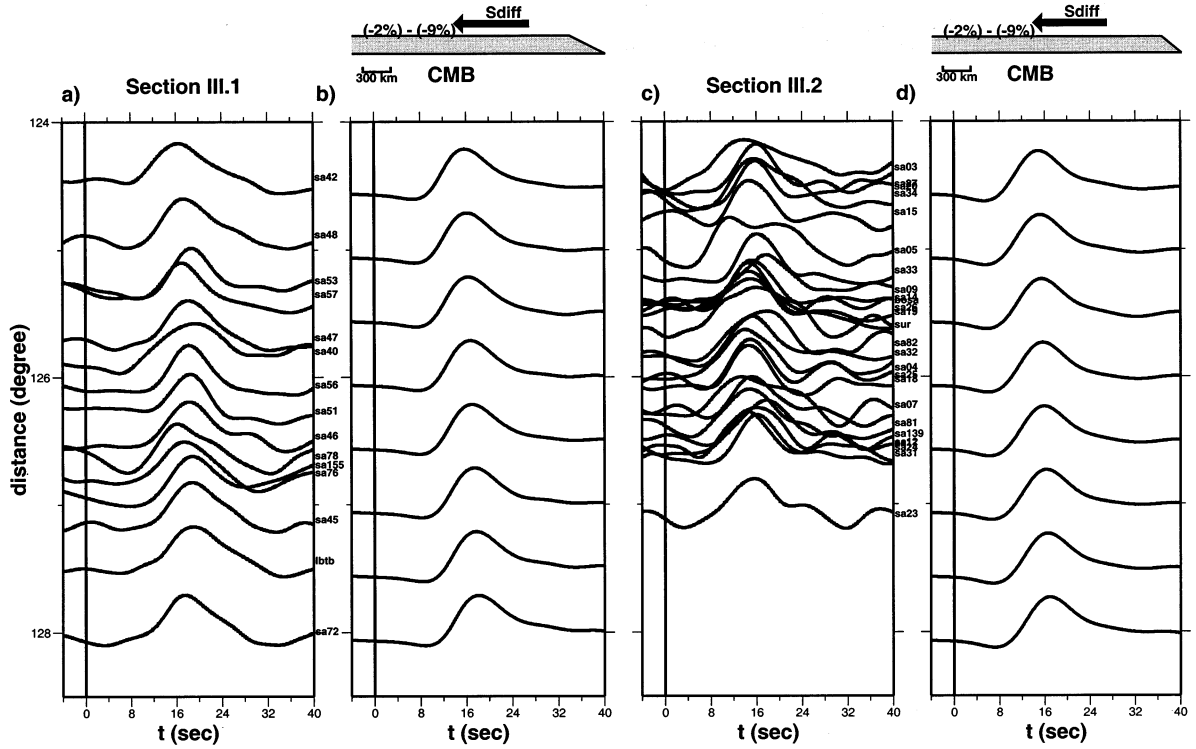


Fig. 5. Observed tangential displacements (a, c) and synthetics (b for a, d for c) for event 98/07/16 (III) (see Fig. 1a for geographic locations of sections III.1 and III.2). Traces are aligned along their theoretical predicted direct SH arrivals ($t=0$) based on PREM. Synthetics are calculated using 200 km (b) and 180 km (d) thick layers with a negative velocity gradient from −2% (top) to −9% (bottom). Model geometries are plotted at the top of panels b and d. The model for section III.1 (b) is the same as that for section II.2 (Fig. 3d), whereas the model for section III.2 (d) is the same as model a for section IV.1 (Fig. 6b). Because of the noise level in high frequencies, all traces are bandpassed from 0.008 Hz to 0.1 Hz.

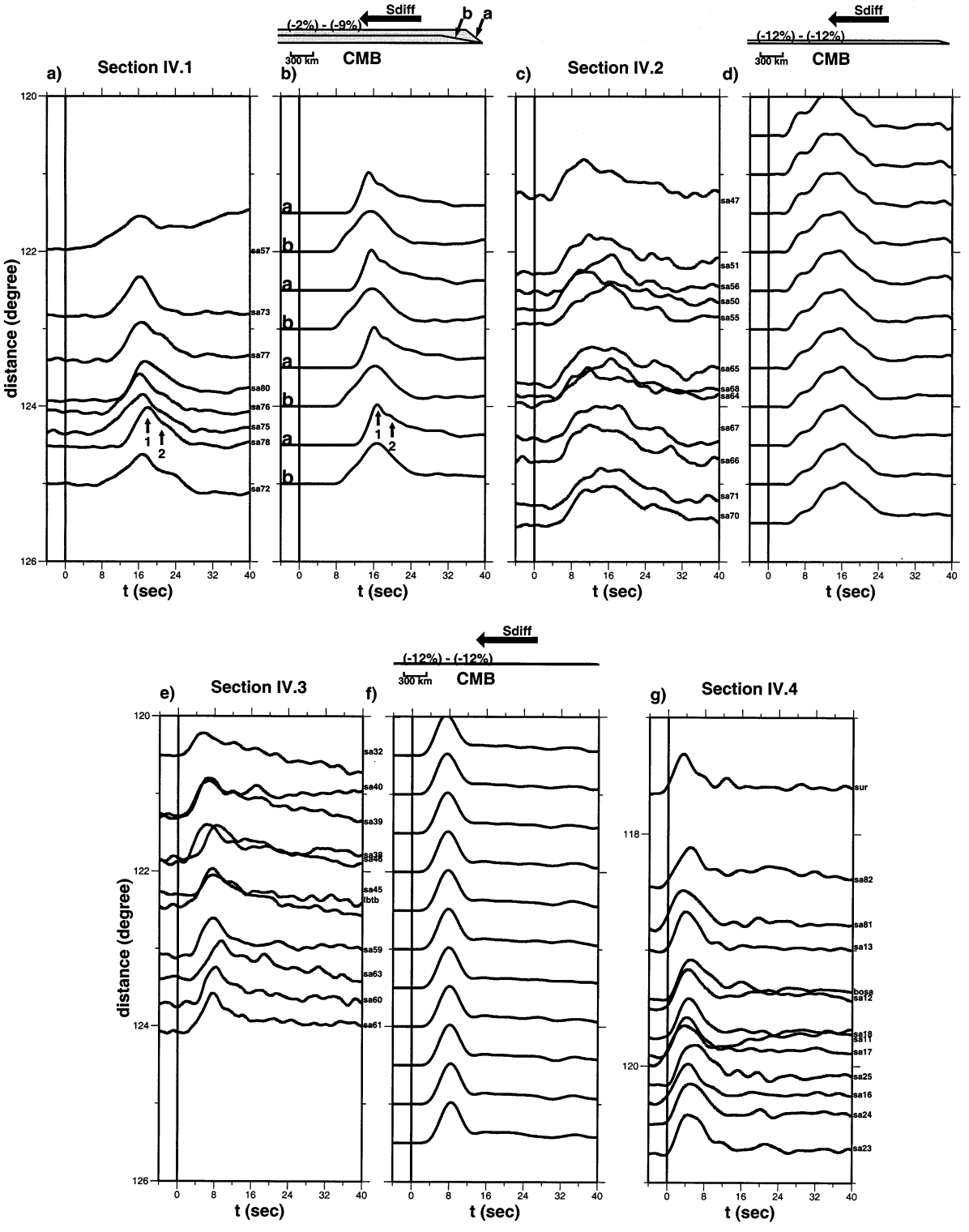
a)
Section IV.1
b)
Sdiff
(-2%) - (-9%)
b a
300 km
CMB
c)
Section IV.2
d)
Sdiff
(-12%) - (-12%)
300 km
CMB
distance (degree)
t (sec)
sa57
sa73
sa77
sa80
sa76
sa75
sa78
sa72
sa47
sa51
sa56
sa50
sa55
sa65
sa68
sa64
sa67
sa66
sa71
sa70
e)
Section IV.3
f)
Sdiff
(-12%) - (-12%)
300 km
CMB
g)
Section IV.4
sa32
sa40
sa39
sa45
lbtb
sa59
sa63
sa60
sa61
sur
sa82
sa81
sa13
sa12
sa17
sa25
sa16
sa24
sa23

Fig. 6. Observed tangential broadband displacements (a, c, e, g) and synthetics (b for a, d for c, f for e) for event 97/09/04 (IV) (see Fig. 1a for geographic locations of sections IV.1, IV.2, IV.3 and IV.4). In panel b, synthetics are presented for two models with different dipping edges and thicknesses, with synthetics and models labeled accordingly. Synthetics for the observations in northern stations (sa73, sa77, sa80, sa78) are calculated using an 180 km thick layer with a negative velocity gradient from −2% to −9% (b, model and synthetics labeled as a), and those for the observations in southern stations (sa57, sa76, sa75 and sa72) are calculated using a 100 km thick layer with a same negative velocity gradient (b, model and synthetics labeled as b). Synthetics in panels d and f are calculated using models with a shear velocity reduction of −12% and a thickness of 37 km and 10 km, respectively. Traces are aligned along their theoretical predicted direct SH arrivals ($t = 0$) based on PREM. Model geometries are plotted at the top of panels b, d, and f.
←

The seismic model in section III.2 is the same as that for the northern part of section IV.1, which is tightly constrained by the seismic observations recorded in northern stations (sa73, sa77, sa80 and sa78) of section IV.1. The tangential displacements observed in these northern stations show a travel time delay of 14 s, pulse-like first arrivals, and a triplicated phase (phase 2) (Fig. 6a). The sharp onsets of direct arrivals and the existence of the triplicated phase are consistent with a combination of a steeply dipping edge and a large negative velocity gradient (Fig. 6b, model and synthetics labeled as a, and see also Fig. 4). On the other hand, the tangential displacements observed in southern stations (sa57, sa76, sa75 and sa72) exhibit gradual onsets of first arrivals, broadening of waveform, and smaller travel time delays (Fig. 6a). The observed features are consistent with a shallower edge dip and a reduced thickness of the anomaly (Fig. 6b, model and synthetics labeled as b). The displacements recorded in section IV.2 show a large decrease of travel time delays and a dramatic change of waveform features with many phases constituting a long-period component (Fig. 6c). For the same reasons we discussed for section II.1, the existence of these multiple phases requires large shear velocity reductions at the base of the mantle and the observed travel time delays require that the low velocity anomaly in this section be confined in the bottom 37 km of the mantle. Indeed, the observed waveforms and travel times place tight constraints on the thickness and the velocity reduction of the layer. They can be explained with a basal 37 km thick layer with a shear velocity reduction of −12% (Fig. 6d), the same value as obtained for section II.1. The wave propagation in this situation is similar to that of the surface Love wave within the low velocity continental crust. Some observations have slightly sharper onsets than synthetics (Fig. 6c). This can be explained with a slightly different model geometry. I do not further explore models to explain each individual trace. The displacements sampling section IV.3 show a travel time delay of 2–3 s and simpler waveforms (Fig. 6e). With a shear velocity reduction of −12%, as those tightly constrained in sections II.1 and IV.2, a 10 km thick basal layer can explain both the travel times and waveforms well (Fig. 6f). The observations sampling section IV.4 show small travel time delays and simple waveforms (Fig. 6g), suggesting the disappearance of the anomaly in this section and confirming the simple source time function of the earthquake.

The SKS travel time observations indicate that the seismic anomaly extends at least to southeast of southern Africa, but only below 32°S latitude (Fig. 1b). The transition from the anomaly to the surrounding mantle around (32°S, 35°E) is also rapid (Fig. 1b). The above detailed waveform modeling results, in conjunction with the observed SKS travel times, allow me to construct a three-dimensional distribution of this anomaly (Fig. 7).

There are small travel time variations associated with this seismic anomaly for the compressional Pdiff phases. The lack of Pdiff travel time delays is consistently observed for all four events. I show an example of Pdiff observations for event 97/09/04 (IV) in Fig. 8. Note that small travel time delays for Pdiff waves are observed across the seismic array for this event, in contrast to the large travel time delays (section IV.1, Fig. 6a) and the rapid variations of travel time delays (sections IV.1, IV.2, IV.3, IV4, Fig. 6a,c,e,g) observed for SHdiff phases. The observed Pdiff travel time delays can be used to place bounds on the P velocity gradient within this seismic anomaly. The compressional velocity gradient needs to be less

than −3% across the 200 km layer from the Pdiff travel time observations.

## 3. Interpretations and implications

The steeply dipping edges, the shear velocity reductions, and the maximum P velocity gradient allowed are remarkably similar to those found for the seismic structure in the lowermost mantle beneath the south Atlantic Ocean [18]. In fact, it appears, from SKS travel times (Fig. 1), that the seismic structure revealed here beneath the Indian Ocean is geographically connected to the boundary layer beneath the south Atlantic Ocean. Wen et al. [18] have extensively discussed various proposals for explaining the seismic characteristics observed in the bottom boundary layer beneath

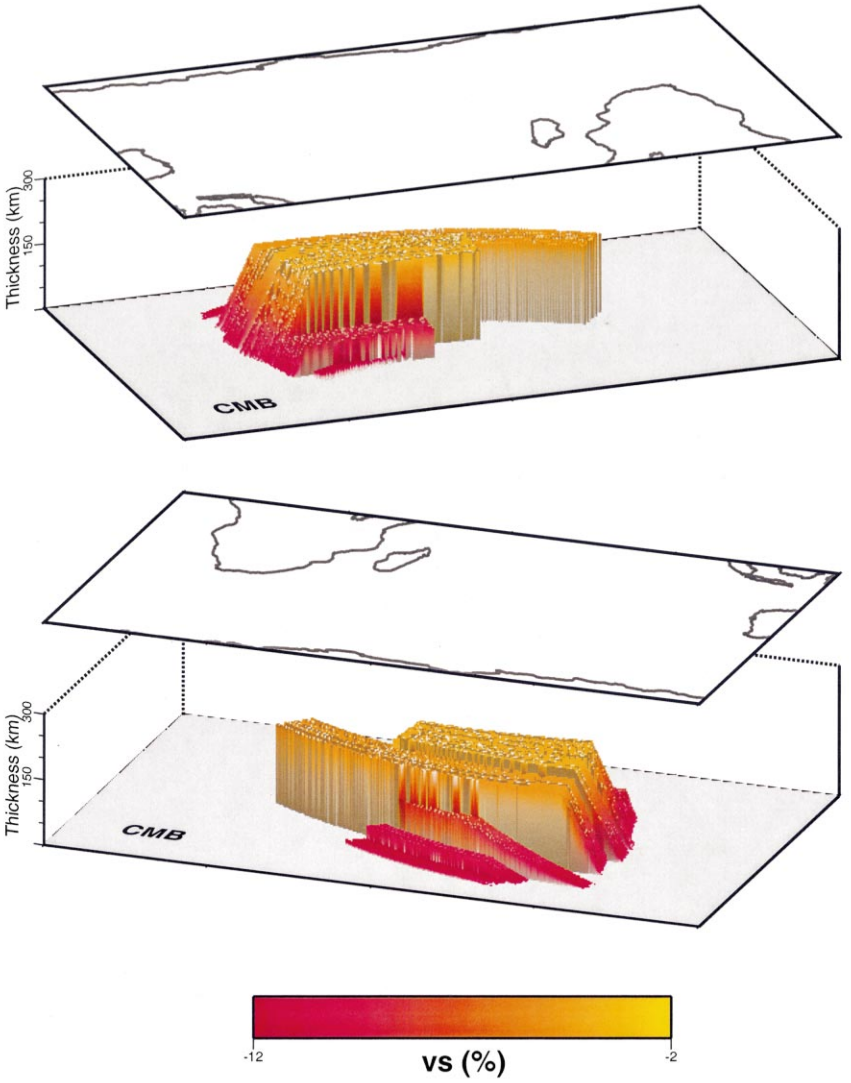


Fig. 7. A three-dimensional model at the base of the mantle beneath the Indian Ocean, with the top panel viewed from 20°N and the bottom panel from 160°N. This model is constructed based on the waveform modeling results from section I to section IV (Figs. 2, 3, 5 and 6) and the observed SKS travel time delays (Fig. 1b). The anomaly has shear velocity reductions from −2% (top) to −9% to −12% (bottom).

the south Atlantic Ocean and their difference from those inferred in the other regions of the core–mantle boundary. They suggest the seismic characteristics observed in the seismic boundary layer beneath the south Atlantic Ocean can be best explained by partial melt driven by a compositional change produced early in the Earth's history [18]. They also suggest that a depressed solidus temperature and/or an enrichment of heat-producing elements of a primordial anomaly explain why the seismic anomaly is preferentially partially molten [18]. For the seismic structure beneath the Indian Ocean, however, the seismic observations also reveal rapid variations of thickness and geometry of the seismic anomaly (Fig. 7) and these seismic characteristics unambiguously confirm the requirement of a compositional change for the seismic anomaly.

The arguments documented in Wen et al. [18], for a chemical anomaly produced early in the Earth's history, apply equally well to the seismic structures inferred here. I briefly summarize the arguments here. Readers are referred to Wen et al. [18] for the detailed discussions. For an isochemical mantle, partial melt is required to explain the magnitude of those shear wave velocity perturbations. Partial melt in an isochemical mantle, however, has difficulties in explaining the geometry and the rapid variations of geometry of the seismic structure. It also cannot consistently explain the seismic structures in other regions of the core–mantle boundary, for example, that beneath the central Pacific. For a chemically heterogeneous mantle, a chemical anomaly produced by the core–mantle reaction or segregation of subduction oceanic crust would not likely explain the unique presence and the steeply dipping edges of this anomalous structure. On the other hand, a chemical anomaly produced by primordial differentiation processes early in the Earth's history not only readily explains the steeply dipping edges, the rapid variations of geometry and thickness, and the unique presence of the anomalous layer, but also provides a feasible physical mechanism for the regional partial melting. The following two characteristics of such a chemical anomaly should significantly affect its melting behavior: (1) it may be enriched in less compatible elements (e.g., Al, Fe, Ca) and perhaps some volatile components. These elements could significantly depress the melting temperature locally; (2) it may also be enriched in heat-producing incompatible elements, such as U, Th, K. Internal temperature may be so elevated due to radiogenic heating that it sustains the partial melting or re-melts locally. In this partial melt scenario, the seismic velocity anomaly represents a partial melting region defined by its distinct composition and the strong shear velocity reductions inside the seismic anomaly reflect different fractions of melt and different temperatures (both increase toward the core–mantle boundary) at different depths of a thermal gradient at the bottom of the mantle.

My results may have significant implications for the geochemistry observed at the surface of the Earth. Dupré and Allègre first noticed that lavas from ocean islands in the south Atlantic and Indian oceans have high $^{87}Sr/^{86}Sr$ ratios and anomalously high $^{207}Pb/^{204}Pb$ and $^{208}Pb/^{204}Pb$ ratios for

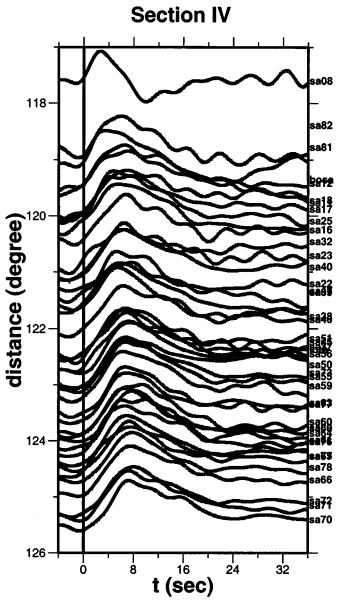


Fig. 8. An example of vertical broadband displacements recorded in the southern African array for event 97/09/04 (IV). All traces are aligned along theoretical predicted arrivals of the Pdiff phase. Note the small travel time delays observed across the array and see Fig. 6 for the SHdiff travel time delays in different sections of this event.

a given $^{206}Pb/^{204}Pb$ ratio [23]. Hart terms this isotope signature and its geographical distribution on the ocean floor the 'DUPAL anomaly' [24]. He also suggests that the isotope data indicate that the DUPAL anomaly is related to very early ($>3$ Gyr) development of enrichment of incompatible elements [24,25]. The geographical correlation between the DUPAL anomaly observed at the surface of the Earth and the compositional anomaly at the bottom of the mantle beneath the south Atlantic Ocean is already documented [18]. Note that the geographical correlation between them in the Indian Ocean is also remarkable, both in the Indian Ocean defined by the Sdiff phases and in the southeast of southern Africa revealed by the SKS travel times (Fig. 1a). The DUPAL maxima for the 90-east ridge are samples of old hotspot traces. The locations of their origin are also geographically within the seismic anomaly at the bottom of the mantle, when the plate motions are taken into account (light blue arrow, Fig. 1a). The proposed origin of this seismic anomaly at the bottom of the mantle, i.e., an enriched chemical anomaly produced early in the Earth's history, is also in line with the early development of enrichments of the DUPAL anomaly suggested by the isotope data. This anomalous compositional anomaly near the core–mantle boundary could provide an explanation for the DUPAL anomaly observed at the Earth's surface, in terms of its geographical distribution, uniqueness and enrichments, if mantle flow or plume is able to entrain the anomalous materials from this bottom compositional layer and carry them to the Earth's surface.

## 4. Conclusions

I report seismic observations of S, ScS, Sdiff, SKS and Pdiff phases sampling the lowermost mantle beneath the Indian Ocean. The observations recorded in the Kaapvaal seismic array for four earthquakes in the Fiji subduction zone provide a good sampling coverage for the lowermost mantle beneath the Indian Ocean and bracket the emergence of a seismic anomaly in the north and its disappearance in the south. These seismic observations show rapid variations of travel time and waveform across small epicentral distances for SH and Sdiff phases, and small travel time delays for Pdiff phases.

From extensive waveform modeling and travel time analysis, I am able to constrain not only the velocity variation and geometry, but also the geographic extent and variation of this seismic anomaly. This low velocity anomaly has steeply dipping edges, rapidly varying thicknesses and geometries, and anomalously low shear wave velocities decreasing from $-2\%$ at 200 km above the core–mantle boundary to $-9\%$ to $-12\%$ at the core–mantle boundary. These seismic and structural characteristics unambiguously suggest that it is a compositional anomaly and its velocity structures can be well explained by partial melt driven by the compositional change within the anomaly. A depressed temperature and/or an enrichment of heat-producing elements of a primordial anomaly explain the localized partial melting. This chemical anomaly geographically coincides with the DUPAL geochemical anomaly in island volcanoes around the Indian Ocean and may provide an explanation for its distinctive isotope characteristics observed at the Earth's surface.

## Acknowledgements

The seismic data used in this paper were collected as part of the Kaapvaal research project. Special thanks go to David James, Paul Silver, Tim Grove, Tom Jordan, Rebecca Saltzer, Rod Green, Sue Webb, Jock Robey, Eddie Kostlin, Maggie Jutz and all participants (http://www.soliduscIw.edu/kaapvaal) for their invaluable contributions to the success of the project. Throne Lay and Barbara Romanowicz provided constructive reviews, which improved the paper significantly. I also thank Saad Haq for assistance in digitizing DUPAL maps. This work is supported by an NSF Grant EAR0001232.*[RV]*

## References

[1] G.F. Davies, Geophysical and isotopic constraints on

mantle convection: an interim synthesis, J. Geophys. Res. 89 (1984) 6017–6040.
[2] L. Wen, D.L. Anderson, Present-day plate motion constraint on mantle rheology and convection, J. Geophys. Res. 102 (1997) 24639–24654.
[3] P.J. Tackley, Three-dimensional simulations of mantle convection with a thermo-chemical basal boundary layer: D″? in: M. Gurnis, M.E. Wysession, E. Knittle, B. Buffet (Eds.), The Core–mantle Boundary Region, vol. 28, Geodynamics, Am. Geophys. Union, Washington, DC, 1998, 231–253.
[4] A.W. Hofmann, Mantle geochemistry: the message from oceanic volcanism, Nature 385 (1997) 219–228.
[5] B.H. Hager, R.W. Clayton, Constraints on the structure of mantle convection using seismic observations, flow models, and the geoid, in: W.R. Peltier (Ed.), Mantle Convection, Gordon and Breach, Newark, NJ, 1989, pp. 657–764.
[6] L. Wen, D.L. Anderson, Layered mantle convection: A model for geoid and topography, Earth Planet. Sci. Lett. 146 (1997) 367–377.
[7] L.H. Kellogg, B.H. Hager, R.D. van der Hilst, Compositional stratification in the deep mantle, Science 283 (1999) 1881–1884.
[8] R.D. van der Hilst, H. Karason, Compositional heterogeneity in the bottom 1000 kilometers of Earth's mantle: Toward a hybrid convection model, Science 283 (1999) 1885–1888.
[9] T. Lay, Q. Williams, E.J. Garnero, The core–mantle boundary layer and deep Earth's dynamics, Nature 392 (1998) 461–468.
[10] M.E. Wysession, A. Langenhorst, M. Fouch, K.W. Fischer, G.I. Al-Eqabi, P.J. Shore, T.J. Clark, Lateral variations in compressional/shear velocities at the base of the mantle, Science 284 (1999) 120–125.
[11] M. Ishii, J. Tromp, Normal-mode and free-air gravity constraints on lateral variations in velocity and density of Earth's mantle, Science 285 (1999) 1231–1236.
[12] G. Masters, G. Laske, H. Bolton, A. Dziewonski, in: S.-I. Karato et al. (Eds.), Earth's Deep Interior: Mineral Physics and Tomography from the Atomic to the Global Scale, AGU Geophys. Monogr., 113, Am. Geophys. Union, Washington, DC, 2000, pp. 63–87.
[13] E. Knittle, R. Jeanloz, Earth's core–mantle boundary: results of experiments at high pressures and temperatures, Science 251 (1991) 1438–1443.
[14] B.A. Buffett, E.J. Garnero, R. Jeanloz, Sediments at the top of the Earth's core, Science 290 (2000) 1338–1342.
[15] E.J. Garnero, R. Jeanloz, On the fuzziness of the core–mantle boundary, Geophys. Res. Lett. 27 (2000) 2777–2780.
[16] J.S. Resovsky, M.H. Ritzwoller, Regularization uncertainty in density models estimated from normal mode data, Geophys. Res. Lett. 26 (1999) 2319–2322.
[17] B. Romanowicz, Can we resolve 3D density heterogeneity in the lower mantle?, Geophys. Res. Lett. 28 (2001) 1107–1110.
[18] L. Wen, P. Silver, D. James, R. Kuehnel, Seismic evidence for a thermo-chemical boundary layer at the base of the Earth's mantle, Earth Planet. Sci. Lett. 189 (2001) 141–143.
[19] A. Dziewonski, D.L. Anderson, Preliminary reference Earth model, Phys. Earth Planet. Inter. 25 (1981) 297–395.
[20] L. Wen, An SH hybrid method and shear velocity structures in the lowermost mantle beneath the central Pacific and South Atlantic oceans, J. Geophys. Res., 2001 (in press).
[21] F. Niu, L. Wen, P. Silver, D. James, Sharp lateral transition of seismic velocity at the base of the mantle beneath southwest of southern Africa, EOS, AGU Spring Meeting 82 (2001) S267.
[22] N.A. Simmons, S.P. Grand, Partial melting in the deepest mantle, Geophys. Res. Lett. (2001) (submitted).
[23] B. Dupré, C.J. Allègre, Pb-Sr isotope variation in Indian ocean basalts and mixing phenomena, Nature 303 (1983) 142–146.
[24] S.R. Hart, A large-scale isotope anomaly in the Southern Hemisphere mantle, Nature 309 (1984) 753–757.
[25] S.R. Hart, Heterogeneous mantle domains: signatures, genesis and mixing chronologies, Earth Planet. Sci. Lett. 90 (1988) 273–296.
[26] P. Castillo, The Dupal anomaly as a trace of the upwelling lower mantle, Nature 336 (1988) 667–670.